



JCSDA Quarterly

NOAA | NASA | US NAVY | US AIR FORCE

<https://doi.org/10.25923/c23x-ac34>

IN THIS ISSUE

1 IN THIS ISSUE

1 NEWS IN THIS QUARTER

EMC Contributions to CRTM Development and Validation

Forecast Sensitivity Observation Impact in a Global Reanalysis

Demonstration of C++ Implementation of GNSS-RO Forward Operators

23 MEETING REPORT

2019 IODA Workshop Summary

25 PEOPLE

28 EDITOR'S NOTE

29 SCIENCE CALENDAR

30 CAREER OPPORTUNITIES

NEWS IN THIS QUARTER

EMC Contributions to CRTM Development and Validation

Introduction and Motivation

The Community Radiative Transfer Model (CRTM) developed at the Joint Center for Satellite Data Assimilation (JCSDA) has been applied to the Grid-point Statistical Interpolation (GSI) analysis system for satellite radiance assimilation in the operational Environmental Model Center (EMC) Global Forecast System (GFS) in support of the daily weather forecast, climate prediction, satellite retrieved product generation, and instrument validation/monitoring. The CRTM is a sensor/channel based fast radiative transfer model, capable of simulating (forward modeling) satellite radiance measurements from atmospheric temperature, water vapor, five optional trace gases, five hydrometeor types, various aerosol species, and surface parameters. The tangent-linear, adjoint, and k-matrix models have also been developed based on the forward model. The current GSI assimilates all instruments in clear-sky condition except for the Advanced Microwave Sounding Unit-A (AMSU-A) and the Advanced Technology Microwave Sounder (ATMS) where additional radiances affected by non-precipitating clouds are also assimilated, and all cloudy scenes are assumed to be overcast in the assimilation (Zhu et al., 2016). The microwave (MW) radiative transfer calculation for non-precipitating clouds (liquid water and ice) involves relatively simple emission-only process compared to that for precipitation where complicated multiple-scattering consideration is required. It is crucial to thoroughly investigate the quality and capability of the observation operator before assimilation to prevent aliasing radiative transfer model error into the analysis. Therefore, in preparation for assimilating satellite radiances under multiple scattering conditions, a rigorous evaluation, development, and validation for CRTM under scattering condition over the ocean is undertaken at EMC (Liu et al., 2015). In addition to the observation as the validation metric, the capability of using Radiative Transfer for TOVS (RTTOV) has been added in GSI to have a more consistent and flexible way in comparing radiative transfer models by using the same GFS 6-hour forecast atmospheric and surface fields. The overall performance for Infrared (IR) sensors, such as the Infrared Atmospheric Sounding Interferometer (IASI) under clear-sky condition, had also been reviewed.

Disclaimer: The Manuscript contents are solely the opinions of the author(s) and do not constitute a statement of policy, decision, or position on behalf of NOAA or any other JCSDA partner agencies or the U.S. Government.

**JOINT CENTER FOR SATELLITE
DATA ASSIMILATION**

 5830 University Research Court
College Park, Maryland 20740

 3300 Mitchell Lane
Boulder, Colorado 80301

 Website: www.jcsda.noaa.gov
EDITORIAL BOARD
Editor:

James G. Yoe

Assistant Editor:

Biljana Orescanin

Director:

Thomas Auligné

Chief Administrative Officer:

James G. Yoe

Support Staff:

Sandra L. Claar

Development of Radiative Transfer for Fractional Cloud Coverage

The cloudy scenes are assumed to be overcast in the all-sky assimilation for AMSU-A and ATMS in GSI, and this is not optimal. Even when two fields of view contain the same amount of hydrometeor content, variational cloudiness can cause substantial differences in measured radiances. To further improve the radiance assimilation under the all-sky condition, EMC has contributed in the development of handling fractional coverage in CRTM. As an initial approach, a two-column radiance calculation was developed with four types of cloud overlapping schemes (van Delst et al., 2016). The impact of fractional cloud coverage can exceed 100 Kelvin for high-frequency MW channels. (*Figure 1A*) Currently, the all-sky assimilation of IASI radiances is under investigation (Bi et al., 2016). Ten moisture channels were selected to assimilate under all-sky condition. Initial testing indicates that the simulated brightness temperature (BT) fit to observation (OmF) and the root mean square (RMS) of the OmF for IR channels can be improved by including the fractional

coverage in the radiative transfer calculation as shown in *Figure 1B*. The hydrometeor-weighted cloud overlap scheme (Geer et al., 2009) was used in the calculation.

Validation of CRTM Under All-sky Conditions in the Microwave Spectral Range

At MW frequencies, the precipitation particles interact with radiation extensively through multiple-scattering processes. The default radiative transfer solver to handle electromagnetic scattering by particles is the Advanced Doubling-Adding (ADA) method with angular dependence of radiation propagation (Liu et al., 2006). The validation of CRTM under all-sky condition shows that the calculated BTs have systematic biases for surface sensitive channels at locations where the ADA solver is involved. (*Figure 2A*) It was discovered that the off-diagonal terms of the surface reflectivity matrix are zero so that there is no diffuse radiation being reflected toward the viewing direction. Due to the lack of a proper surface reflectivity model for multiple-scattering radiative transfer, a workaround has been developed

Figure 1. The impact of using overcast assumption and fractional cloudiness: (A) BT difference for MHS 157 GHz channel; (B) bias and RMS of OmF for the ten selected IASI moisture channels (2889, 2958, 2993, 3002, 3049, 3105, 3110, 5381, 5399, 5480).

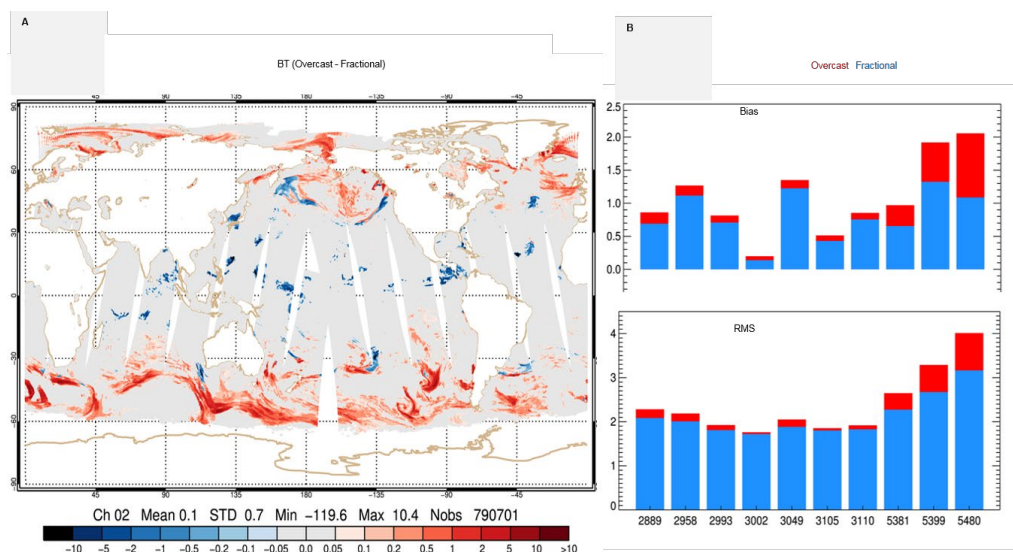
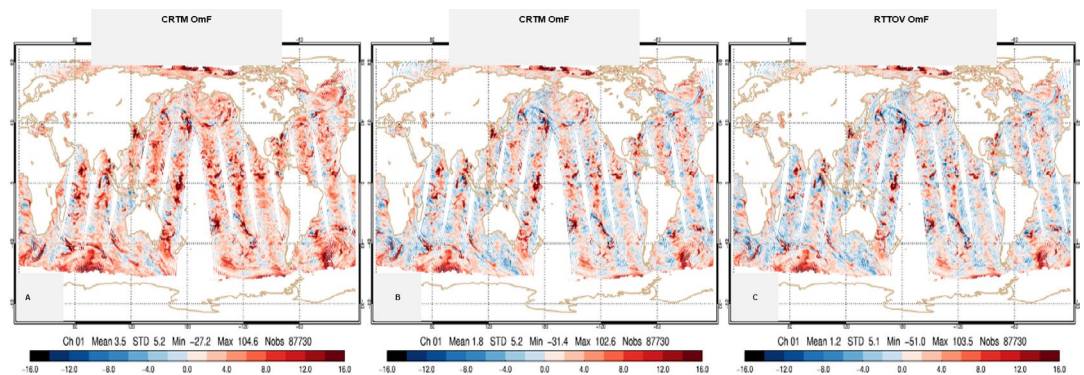


Figure 2. The simulated brightness temperature fit to observation for AMSU-A channel 1 using: (A) CRTM release prior to v2.3.0, (B) CRTM release v2.3.0, and (C) RTTOV v11.3.



at EMC to reduce the bias by including the reflection correction (Deblonde and English, 2000), in conjunction with the ADA solver, and has been incorporated into CRTM v2.3.0 release. As a result, the calculated AMSU-A BTs with the workaround show significant improvement in accuracy as compared to the observation (*Figure 2B*) and the BTs calculated from RTTOV (*Figure 2C*), respectively. Ultimately, a more physical approach, such as the bidirectional reflectance distribution function (BRDF) over the ocean for MW sensors, is currently under development at JCSDA.

The improvement in simulated BTs with the workaround (reflection-correction fix) for surface sensitive channels can be seen in all other MW sensors. The BT fit to observation for GMI and AMSU-A is shown in *Figure 3A* and *3B*, respectively. There is an anomaly in the statistics for the 52 GHz channel that the bias is worse after the fix. In fact, the global

maps of innovation of this channel indicate that the inclusion of the surface reflection correction reduces the biases significantly. (*Figures 3C* and *3D*) It is the canceling effect of the positive and negative biases that gives the impression the biases are smaller before the fix.

Another issue found in using CRTM under the scattering condition for MW, by comparing the lower panels of *Figure 4A* and *4B* for ATMS, is that the surface emissivity Jacobians exhibit opposite signs for surface sensitive channels as compared to those from RTTOV using the same forecast model profiles. While the temperature Jacobians are mostly consistent between CRTM and RTTOV, the CRTM response of brightness temperature to the surface temperature change seems unphysical. The increase in surface emissivity should result in an increase in brightness temperature in these channels.

Figure 3. The innovation statistics: (A) bias and RMS of GMI channels; (B) bias and RMS of AMSU-A channels. The global maps of innovation for AMSU-A 52 GHz channel (C) without and (D) with the reflection correction fix.

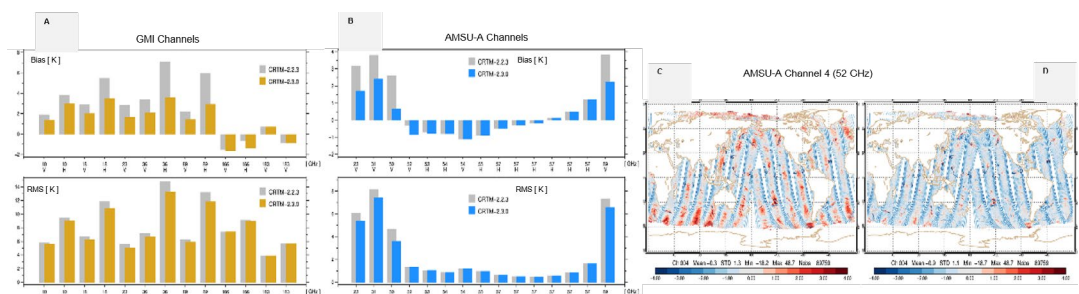
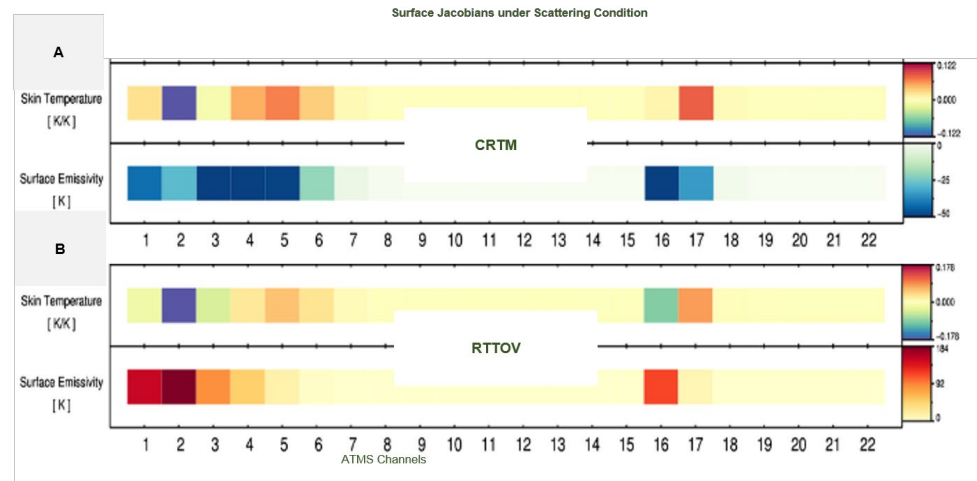


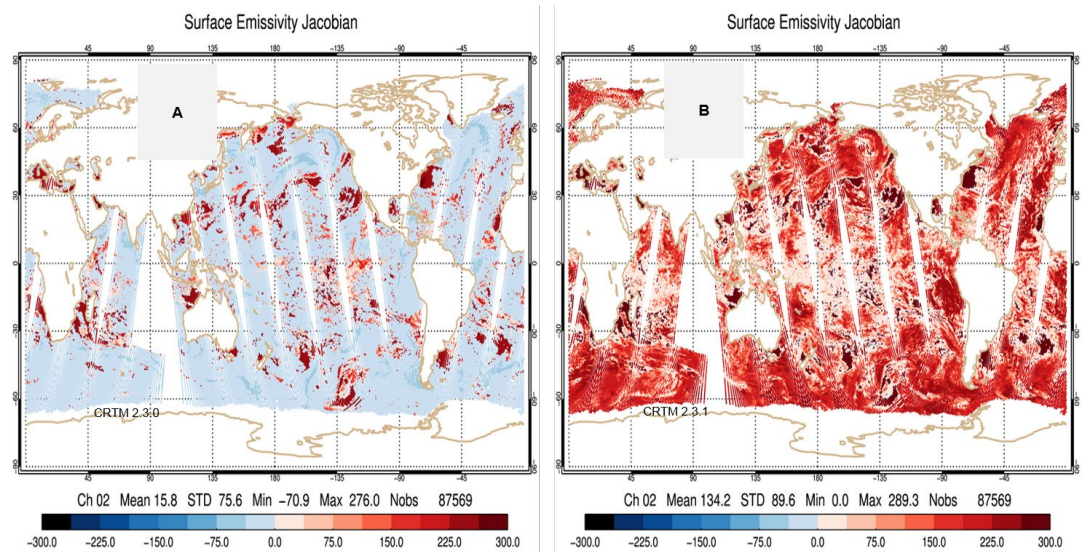
Figure 4. Surface temperature and emissivity Jacobians from (A) CRTM and (B) RTTOV under scattering condition for ATMS Channels.



Upon investigating the CRTM code, the unphysical response in surface emissivity Jacobian appeared to be a coding error in the output module of CRTM, not an error in the radiative transfer algorithm or surface emissivity model. The correction of the coding error will be included in the next release of CRTM (v 2.3.1). The surface emissivity Jacobians for AMSU-A channel 2 before and after the coding fix are shown in *Figures 5A* and *5B*, respectively. It is worth noting that this coding error for surface emissivity Jacobian has a significant impact

on radiance assimilation under scattering conditions, and this is because the surface emissivity Jacobians are used in quality control, observation error adjustment, and bias correction. The error in surface emissivity Jacobians will not only result in 20% fewer data passing quality control, but also result in less optimal observation error assignment and bias correction estimation. It is advisable that users of CRTM with versions prior to the 2.3.1 release performing all-sky radiance assimilation should revisit their results.

Figure 5. Surface emissivity Jacobians for AMSU-A channel 2 calculated from CRTM (A) v2.3.0 and (B) v2.3.1.



Validation of CRTM Under Clear-sky Conditions in the Infrared Spectral Range

Before diving into the validation for IR under the all-sky condition, validation under the clear-sky condition for IASI was conducted first. The validation was based on one month of operational GFS 6-hour forecast fields. The RMS of the brightness temperature difference between CRTM and RTTOV shown in *Figure 6A* indicates a moderate difference in surface and moisture sensitive channels, a large discrepancy in solar affected channels, and a spike in one channel that has a strong sensitivity to both CH₄ and N₂O gases. The RMS of brightness temperature fit to observation between CRTM and RTTOV provides an objective measure of which RTM generated brightness temperatures fit closer to observations as shown in *Figure 6B*, in which three distinct features (marked as A, B, and C respectively) can be observed. Firstly, the CRTM simulates moisture channels fit better than RTTOV (marked as a in *Figure 6B*), and the monthly averaged biases for moisture channel at wavelength 1498.75 cm⁻¹ from CRTM and RTTOV shown in *Figure 7A* indicate the CRTM generally outperforms RTTOV in IASI moisture channels. While RTTOV uses the Optical Depth at Pressure

Space (ODPS) transmittance model for all gaseous absorption, CRTM uses Optical Depth at Absorber Space (ODAS) for water vapor absorption and OPDS for all other gases. Early studies showed that using water vapor amount instead of pressure level can improve the accuracy in the transmittance calculation (Chen et al., 2010). Secondly, CRTM has a significant bias in simulating the channel with strong absorption of CH₄ and N₂O together (marked as B in *Figures 6B* and *7B*), and this indicates a problematic prediction of optical depth for channels sensitive to these trace gases. Lastly, a systematic bias in CRTM is observed across the window and surface sensitive channels (marked as C in *Figure 6B*). CRTM consistently overestimates the brightness temperatures, especially in polar regions as compared to observations and estimates from RTTOV. (*Figure 7C*) The overestimate in BT may result from an overestimate in surface emissivity estimation. The difference in surface emissivity between CRTM and RTTOV (*Figure 8A*), confirms the hypotheses that the surface emissivity values from CRTM are consistently higher than those from RTTOV and thus result in overestimated BT values in IASI surface sensitivity channels. The biases in surface emissivity from CRTM

Figure 6. IASI channel statistics: (A) RMS of brightness temperature differences between CRTM and RTTOV; (B) differences between the RMS of OmF from RTTOV and the RMS OmF from CRTM.

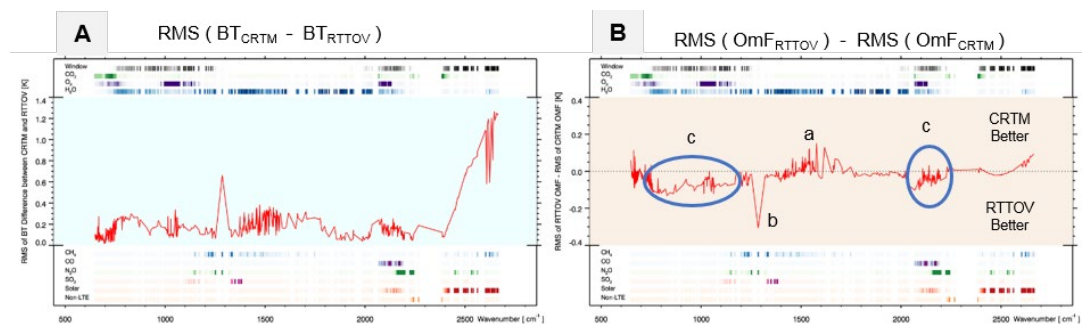


Figure 7. Monthly averaged OmF for CRTM (left panel) and RTTOV (right panel) at three IASI wavelengths: (A) 1498.75 cm⁻¹, (B) 1285.25 cm⁻¹, and (C) 801 cm⁻¹.

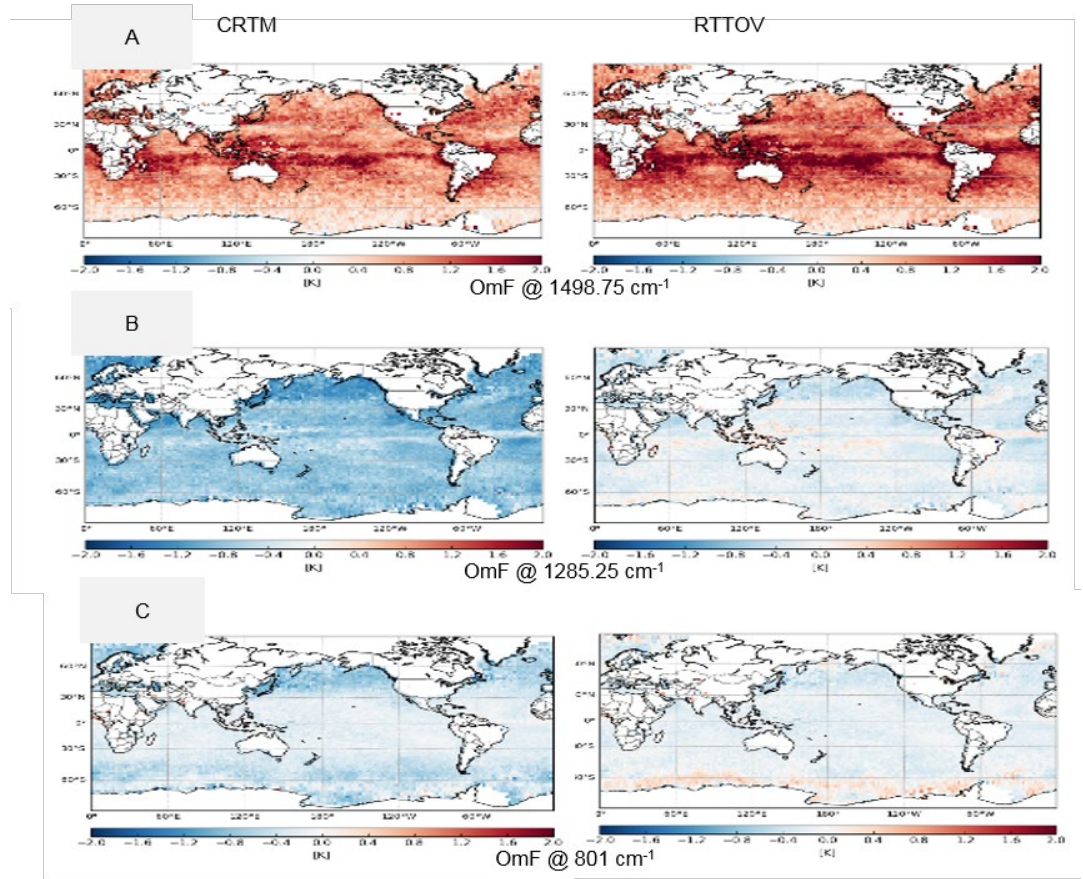
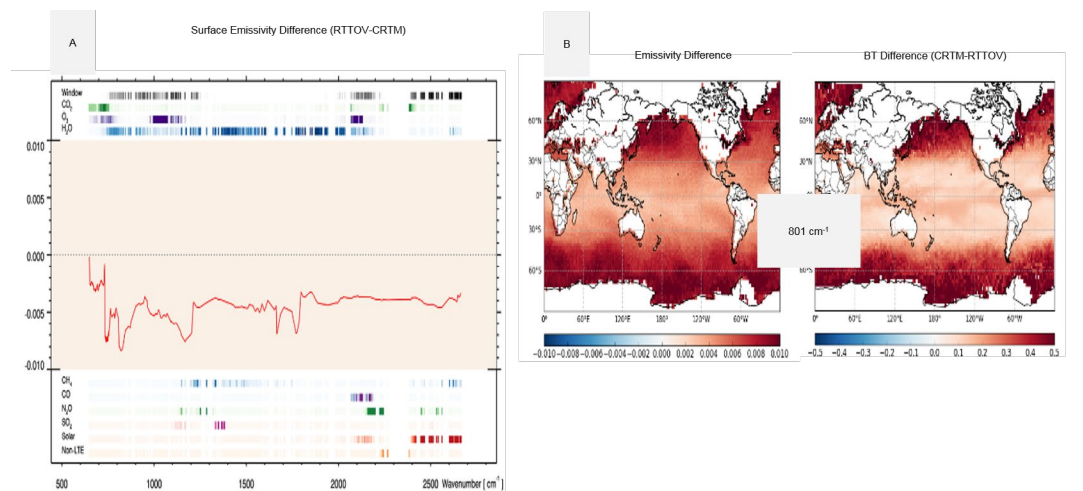


Figure 8. (A) IASI Channel dependence of surface emissivity difference between CRTM and RTTOV; (B) CRTM-RTTOV difference for surface emissivity (left) and BT (right) for IASI.

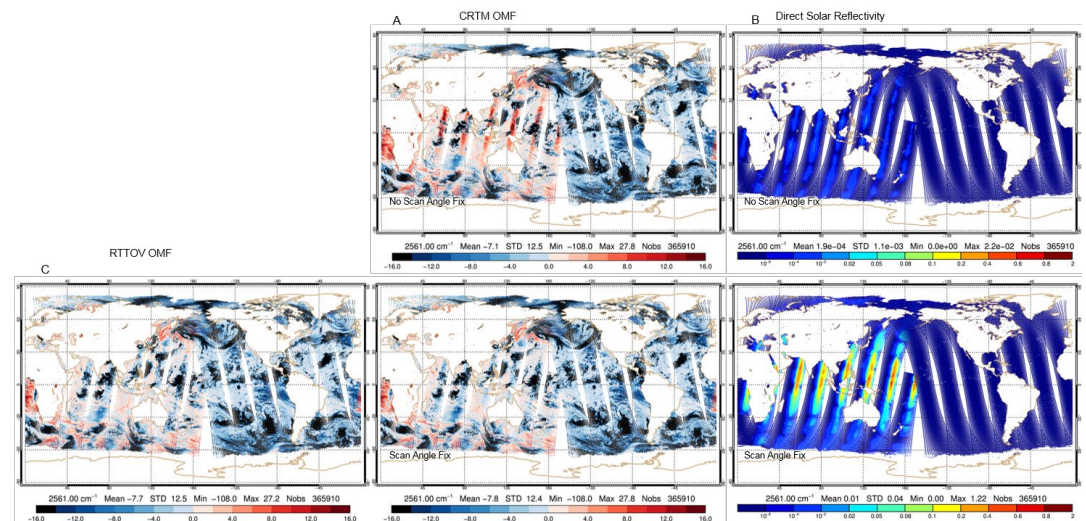


and the corresponding biases in brightness temperature show latitude dependence and are increasing towards polar regions. (Figure 8B) A closer investigation in the Infrared Sea Surface Emissivity Model (IRSSEM) used in CRTM found that the emissivity is parameterized in terms of zenith angle and wind speed only. However, there is evidence that the skin temperature-dependent refraction indices in the window channels also play an essential role in determining surface emissivity (e.g., Newman et al., 2005; Nalli et al., 2008). As a result of the current study, there is a renewed effort at the National Environmental Satellite, Data and Information Service (NESDIS) to include the skin temperature-dependent refraction indices in the model for training the regression-based IRSSEM with additional skin temperature predictor.

In solar-affected IASI channels, the discrepancy between CRTM and RTTOV is significant. (Figure 6A) The main difference in BT estimation in these channels comes from the daytime part of the globe as shown

in the upper panel of Figure 9A, and the differences are more significant at smaller solar zenith angles. While the direct solar radiance is the major part of the radiance toward satellite view angle, the direct solar reflectivity estimated from BRDF seems too small (upper panel in Figure 9B), and this is found to be a misuse of satellite zenith angle as input to CRTM, which requires the sensor zenith angle ranging from zero to its maximum zenith angle. However, the sensor zenith angle was set to negative if the footprint number is smaller than that for nadir, and thus resulted in a much underestimated direct solar reflectivity, as well as brightness temperature. With the correct input of sensor zenith angle to CRTM, the estimated direct solar reflectivity from BRDF results in a more reasonable direct solar reflectivity (lower panel in Figure 9B) and a better simulation in brightness temperature for solar-affected region as compared to the observation (lower panels in Figures 9A) and the simulation from RTTOV. (Figure 9C)

Figure 9. (A) CRTM OmF; (B) direct solar reflectivity before (upper) and after (lower) the scan angle fix; (C) RTTOV OmF for IASI wavelength at 2561cm-1.



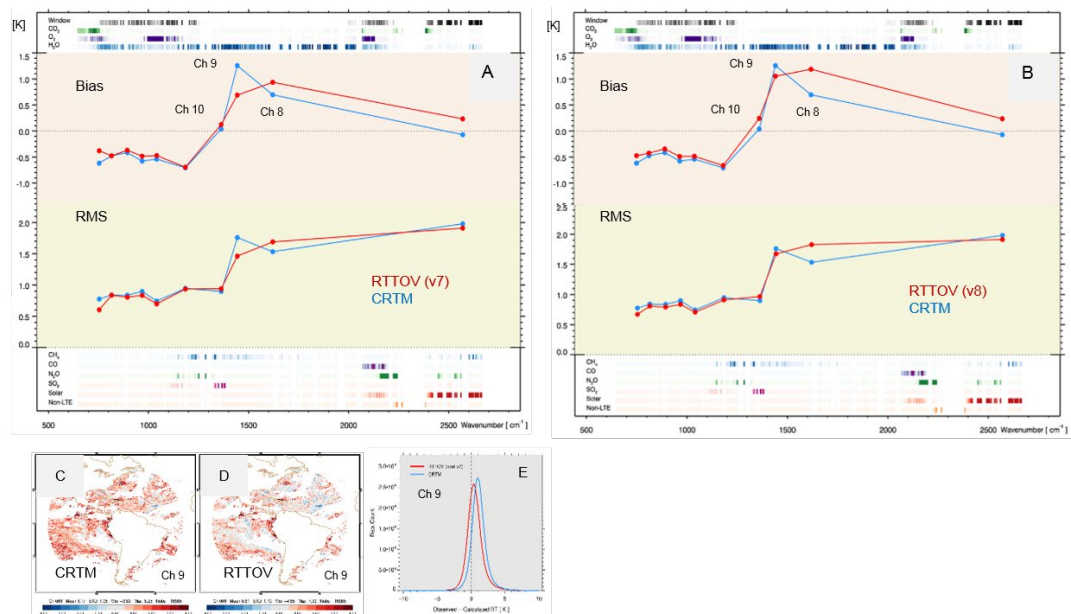
While preparing for radiance assimilation from the Advanced Baseline Imager (ABI) sensor on board of GOES-16 and -17, the clear-sky radiance (CSR) product for channels with central wavelengths longer than 3.9 micron (channels 7-16) is currently being investigated. The initial assimilation efforts focus on moisture channels (8-10); therefore, only moisture channels are discussed here. The statistics of simulated brightness temperatures for moisture channel 9 (sensitive to the middle-level water vapor) appears to have larger differences relative to the observations and also relative to RTTOV with v7 predictor coefficients. The biases for channel 9 from CRTM can be 0.6 Kelvin larger than those from RTTOV. (Figures 10A, C, D, and E) As mentioned in the previous section, the CRTM generally outperforms RTTOV in simulating moisture channels due to the use of ODAS transmittance model. Thus, the possible reasons for the larger bias in CRTM for the ABI moisture channel 9 could result from other factors, such as errors in spectral response function or in the process of generating the coefficients. There

is still room for CRTM to improve the ABI simulation and the effort is continuing. It is worth noting that the comparison with RTTOV v8 predictor coefficients for GOES-16 showed that the fit to observations becomes worse, in general, for moisture channels 8-10. (Figure 10B) It is desirable to learn the difference between RTTOV v7 and v8 predictor coefficients and its link to the deterioration in simulating the moisture channels 8-10. The lessons learned may help CRTM in finding and improving its own issues in simulating channel 9.

Plans

EMC will continue to participate in the validation of CRTM and will take part in CRTM development when appropriate. The exercise of the inter-comparison between CRTM and RTTOV in GSI, as reported here, has shown its value in facilitating a more accurate observation operator and verifying whether GSI provides the correct input information to CRTM. The enhancement and improvement in CRTM make it more appropriate in modeling radiative transfer

Figure 10. ABI GOES-16 statistics: (A) mean and RMS of OmF from CRTM and RTTOV v7 coefficients; (B) mean and RMS of OmF from CRTM and RTTOV v8 coefficients; (C) Ch 9 OmF coverage from CRTM; (D) Ch 9 OmF coverage from RTTOV v7 coefficients; (E) Ch 9 OmF Histogram for CRTM (blue) and RTTOV v7 coefficients (red).



under scattering conditions. Currently, the assimilation of precipitation-affected MW radiances and their impact to forecast are under development and investigation. The next validation targets are the IR sensors under the all-sky condition and the short-wave IR channels under clear-sky condition. Besides, the validation will expand to all other surface types. The validation effort will be repeated if any new or updated feature is in the new release.

Authors

Emily Huichun Liu (SRG/NCEP/EMC), Andrew Collard (IMSG/NCEP/EMC), Li Bi (IMSG/NCEP/EMC), Haixia Liu (IMSG/NCEP/EMC), Mingjing Tong (SAIC/GFDL), Jim Jung (CIMSS), Benjamin Johnson (UCAR/JCSDA), Ming Chen (UMD/NESDIS/STAR), Quanhua Liu (NESDIS/STAR), Tong Zhu (IMSG/NESDIS/STAR), and Nicholas Nalli (IMSG/NESDIS/STAR)

References

Bi L, Collard A, Liu EH, Jung J, Derber J. 2016. Towards the assimilation of all-sky infrared radiances for selected humidity-sensitive IASI channels at NCEP/EMC. In Fourth IASI Conference, Antibes Juan-les-Pins, France

Chen Y, Han Y, Van Delst P, Weng F. 2010. On water vapor Jacobian in fast radiative transfer model. *J. Geophys. Res.*, 115, D12303, doi:10.1029/2009JD013379.

Deblonde G, English SJ. 2001. Evaluation of the FASTEM-2 fast microwave oceanic surface emissivity model. In Technical Proceedings of the 11th International TOVS Study Conference, 20 – 26 September. Budapest. ITWG/IAMAS.

Geer AJ, Bauer P, O'Dell CW. 2009. A revised cloud overlap scheme for fast microwave radiative transfer. *J. Appl. Meteorol. Climatol.* **48**:2257–2270.

Liu EH, Collard A, Sun R, Zhu Y, van Delst P, Groff D, Derber J. 2015a. Inter-comparison of CRTM and RTTOV in NCEP Global Model. In 20th International TOVS Study Conference.

Liu Q, Weng F. 2006. Advanced doubling-adding method for radiative transfer in planetary atmospheres. *J. Atmos. Sci.* **63**: 3459–3465. <http://dx.doi.org/10.1175/JAS3808.1>.

Nalli NR, Minnett PJ, Maddy E, McMillan WW, and Goldberg MD. 2008. Emissivity and reflection model for calculating unpolarized isotropic water surface leaving radiance in the infrared. 2: Validation using Fourier transform spectrometers, *Appl. Optics*, **47**(25), 4649-4671.

Newman SM, Smith JA, Glew MD, Rogers SM, Taylor JP. 2005. Temperature and salinity dependence of sea surface emissivity in the thermal infrared, *Q. J. R. Meteorol. Soc.* **131**, 2539-2557.

van Delst, P, Liu EH, Bi L. 2016. Cloud Fraction in the CRTM, JCSDA Office Note CRTM-4, rev 71147.

Zhu Y, Liu EH, Mahajan R, Thomas C, Groff D, van Delst P, Collard A, Kleist D, Treadon R, Derber J. 2016. All-sky microwave radiance assimilation in the NCEP's GSI analysis system. *Mon. Weather Rev.* **144**: 4709–4735. <https://doi.org/10.1175/MWR-D-15-0445.1>.

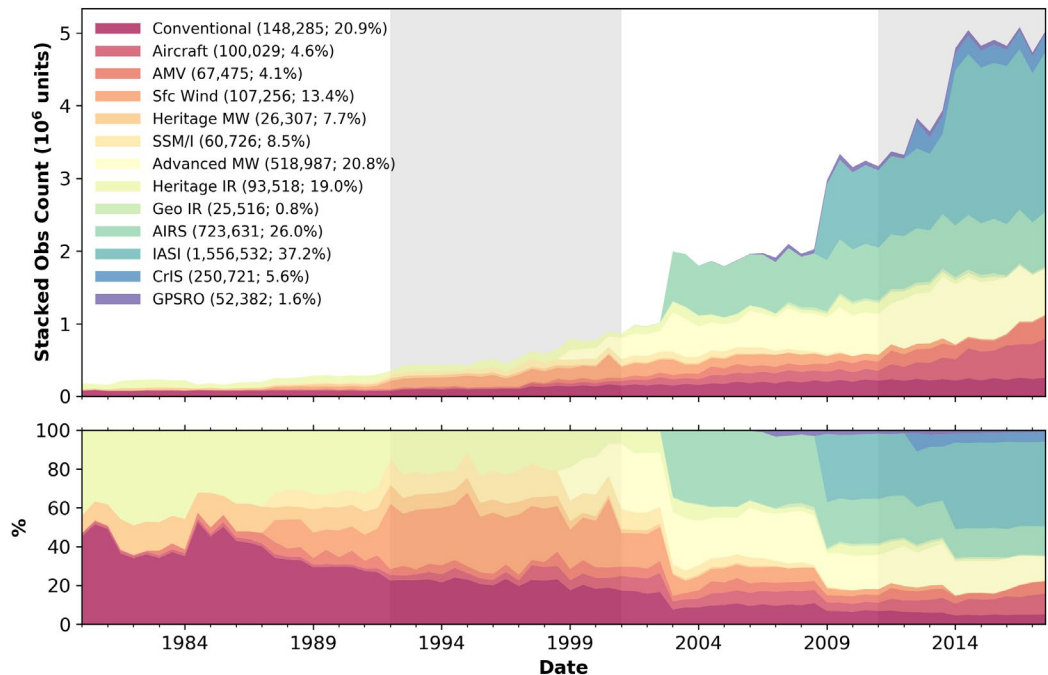
Forecast Sensitivity Observation Impact in a Global Reanalysis

Operational and quasi-operational Numerical Weather Prediction (NWP) centers have been providing routine assessment of the contribution from various observing systems to reducing the error in short-range forecasts for a number of years now. The original technique (Langland and Baker 2004), later termed forecast sensitivity observation impact (FSOI), involves definition of an error metric for the forecasts, typically with respect to verifying analyses, and evaluation of corresponding sensitivities with respect to changes in the observing system that require adjoint operators of both the underlying tangent linear model and the corresponding analysis technique.

FSOI provides a view of how different components of the observing system contribute to forecasts. The present work is an application of FSOI to reanalysis and aims at providing an expanded view of the contribution of various observing systems to the improvement of short-range forecasts over nearly 40 years of assimilation. Typical of reanalysis studies, the investigation benefits from the fact that no system changes occur throughout the course of the reanalysis other than changes in the observing system. In other words, while results from NWP-based studies can be affected by the systematic upgrades to the underlying forecasting model and corresponding analysis system, reanalysis results are not affected by such upgrades since a single version of the model and analysis is used throughout the exercise.

The present study uses GMAO's MERRA-2 (Gelaro et al., 2017) since its software contains all ingredients necessary for FSOI studies. MERRA-2 is a follow up to MERRA (Rienecker et al., 2011) that is primarily aimed at providing an improved water cycle as compared not only to MERRA but also to other available reanalyses. The reader is referred to Gelaro et al. (2017) and various related MERRA-2 documentations for specific details. What is directly relevant to the discussion in this short note is that MERRA-2 atmospheric analysis relies on the Grid-point Statistical Interpolation (GSI) system (Kleist et al. 2009) and ingests a rich diversity of observing systems described in detail in McCarty et al. (2016). *Figure 1* provides a brief summary of the observing systems in the 0000 UTC analyses of all January and July months of MERRA-2 between 1980 and 2017, and follows the instrument partitioning in McCarty et al. (2016) to show: observations of temperature, specific humidity, surface pressure and wind components from surface and upper-air in situ instruments (Conventional); observations of temperature and wind components from aircraft in situ instruments (Aircraft); radiance observations from advanced microwave instruments (Advanced MW, e.g., AMSU-A, AMSU-B, MHS, ATMS); radiance observations from the Atmospheric Infrared Sounder (AIRS); satellite-derived wind components from atmospheric motion vectors technique (AMV); radiance observations from the Cross-track Infrared Sounder (CrIS); infrared radiance observations from geostationary satellites (Geo IR); bending angle observations obtained

Figure 1. Time series of monthly mean stacked observation count (top) and its fractional (bottom) for 0000 UTC analyses during the months of January and July. The vertical shaded and non-shaded areas represent the four streams of MERRA-2. Numerical values in the legend represent the mean number of observations and the mean fractional observation count. The scale factor for observation count is 10^6 .



using the global positioning system radio occultation technique (GPSRO); radiance observations obtained from early infrared instruments (Heritage IR, e.g., SSU, HIRS-2, HIRS-3, HIRS-4) and early microwave instruments (Heritage MW, e.g., MSU); radiance observations from the Infrared Atmospheric Sounding Interferometer (IASI); surface wind from scatterometers (Sfc Wind); and radiance observations from the Special Sensor Microwave Imager (SSM/I). Notice that precipitation and ozone observations are not included in the figure since this work does not provide an estimate of impacts from these data types. The percentage of observations used is displayed in the bottom panel and shows, for example, how Conventional observations amounted to over 45% of the total count of observations available in the beginning of the reanalysis and how this percentage steadily reduces in light of the volume of satellite observations that become available especially from the early 2000s and beyond;

the so-called Earth Observing System (EOS) era. When it comes to count, the recent years are overwhelmingly dominated by the observations from hyperspectral sensors.

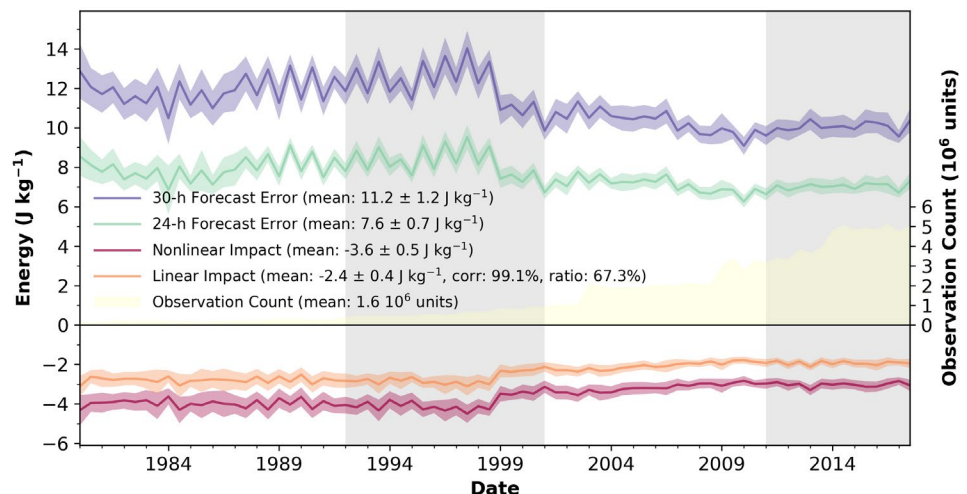
The three necessary ingredients to produce FSOI assessment of the observing system following Langland and Baker (2004) are: the definition of a measure of forecast error, the evaluation of the changes in the forecast due to changes in the corresponding initial conditions (analyses), and the evaluation of the sensitivities in the analysis due to changes in the observations. The forecast error measure used in this work is based on the, now traditional, linearized moist total energy norm. The approach of Langland and Baker (2004) requires the evaluation of this measure for the 24- and 30-hour forecasts and defines error with respect to self-verification; namely, the MERRA-2 analyses. The gradients of each 24- and 30-hour forecast error are fed into the adjoint of the MERRA-2 GEOS general circulation

model (Holdaway et al., 2013) and are integrated for 24 hours. The 24- and 30-hour output forecast sensitivities generated for each analysis cycle of interest are added and provided as input to the adjoint of GSI (Trémolet 2008). It is relevant to point out that forecasts are not a byproduct of MERRA-2. This work involves generating all the required 24- and 30-hour forecasts. Thus, to keep work within bounds, FSOI is only calculated for the 0000 UTC analyses of the months of January and July from 1980 to 2017. This prevents us from making any statements about the daily variability of the impacts but still provides us with a rich amount of information about the contribution of the observing system over the past nearly 40 years.

Figure 2. Time series of 30-h (purple) and 24-h (green) forecast errors, nonlinear (red) and linear (orange) impact estimates and the count of used observations (yellow). Lines represent monthly mean values with ± 1 standard deviation from the mean in shading for 0000 UTC analyses during months of January and July. The vertical shaded and non-shaded areas represent the four streams of MERRA-2. Numerical values in the legend represent mean ± 1 standard deviation in addition to the correlation between linear and nonlinear impacts and its ratio. The units of energy are J kg^{-1} and the scale factor for observation count is 10^6 .

It is instructive to examine the behavior of the (short-range) forecast error over the course of the reanalysis period. *Figure 2* shows the monthly mean 24- (green) and 30-hour (purple) forecast errors evaluated using the total moist energy norm required for FSOI. A one standard deviation variability in the error is shown by the shading around the error curves. There is a clear transition in the errors

in the late 1990s. This has been identified in other works (e.g., Dee and Uppala 2009), and it is attributed to the introduction of high-quality satellite observations. A finite perturbation interpretation of FSOI relates it to the difference between these two error curves. That is, the impact of assimilating observations is related to how much the 30-hour forecast error is reduced by re-issuing the forecast from an analysis available six hours later, when new observations have been assimilated. This forecast error reduction—the so-called *nonlinear* impact—is shown in the figure by the red curve. Just as the forecast errors, this curve too shows a transition in its behavior after the late 1990s. The dramatic change in the observing system is reflected in the consistent reduction of forecast errors from the pre-EOS era into the EOS era. The forecast errors, and corresponding reductions, can be split into regional sections, particularly allowing for better understanding of the impact of assimilation in each hemisphere, as well as in the tropics (not shown). However much of these errors and corresponding forecast sensitivities derived from the adjoint model integration might illustrate (not shown),



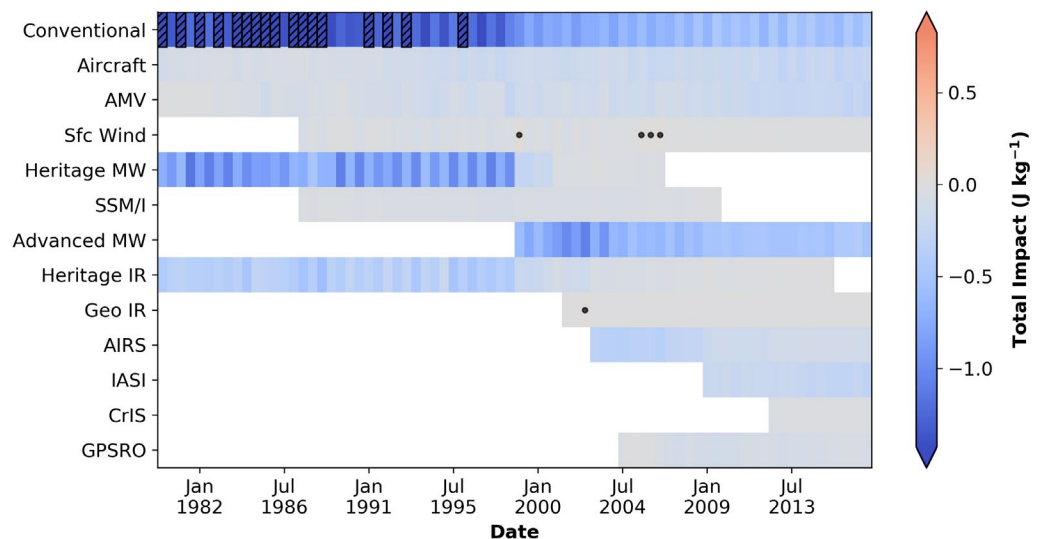
it is not possible to identify from these the contribution of each of the individual components of the observing system.

FSOI is the methodology chosen here to provide this detailed level of quantification—other non-adjoint- and non-ensemble-based techniques also exist (see Todling 2013). FSOI is a calculation in observation-space that approximates the forecast error reduction (red curve) shown in *Figure 2*. A time series of the monthly mean total FSOI over most of the MERRA-2 period is shown in the figure by the orange curve. The level of accuracy of its approximation depends on the accuracy of the representation of the physical processes in the adjoint model, the accuracy of the adjoint analysis, and the resolution at which these adjoints are invoked. In this exercise, forecasts are issued on the 50 km MERRA-2 grid, whereas the adjoint model integrations are produced on the 100 km grid and the adjoint analysis are produced on the 50 km grid. The level of consistency seen between the total nonlinear error reduction and the total FSOI is enough

to allow for examination of the breakdown of the impacts into the various components of the observing system.

A split of the monthly mean observation (linear) impact into the observation categories of *Figure 1* appears in *Figure 3*. Conventional observations undoubtedly contribute consistently to reduce forecast errors. In the beginning of the reanalysis, the dominance of Conventional observations leads the mean impacts that are higher than three standard deviations. Over time, as their availability diminishes and more satellite observations dominate the mix, the impact of Conventional observations reduces, but its contribution remains significant even when the percentage of Conventional observations falls to the single percentage digits in today’s blend of data. The consistent contribution from Microwave remote observations is also noticeable. The contribution from Heritage MW (i.e., MSU) is nicely taken over by introduction of the Advanced MW sensors (largely AMSU-A). Heritage IR (such as SSU and

Figure 3. Heatmap of monthly mean total observation impact for the observation categories of *Figure 1*. Values are for 0000 UTC analyses for the months of January and July. Patched boxes represent values larger than 3 standard deviations from the mean and dots represent boxes with negative values. The units of energy are $J\ kg^{-1}$.

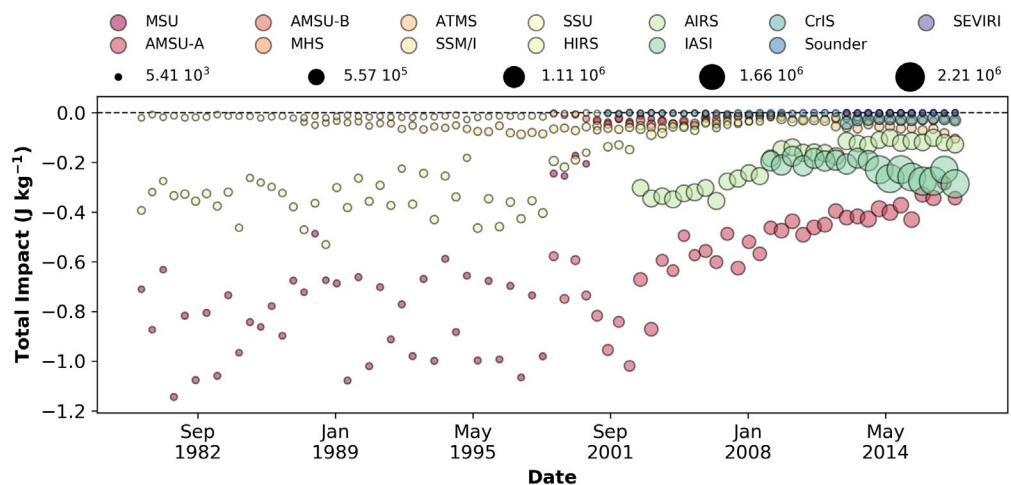


HIRS-2) contributes considerably before the EOS-era; the introduction of hyperspectral instruments (AIRS initially, then IASI and CrIS) tends to steal from the heritage IR instruments (and more). The shading in the figure gives the impression that observations from Aircraft, AMVs, and even GPSRO are of secondary significance. We should recall that some of these observing systems are highly localized, not only horizontally but also vertically, and thus appear to contribute little to a global measure (norm). Therefore, this work must be put in the context of a number of other works evaluating the contribution of individual instruments.

Another way to partition FSOI is to look at the impact of radiance observations obtained from a variety of satellite platforms and instruments. *Figure 4* shows the monthly mean impacts of radiance for the main satellite instruments used in MERRA-2. In the beginning of the reanalysis period, most of the satellite contribution comes from MSU and HIRS. SSU is supposedly a

major contributor in the stratosphere, but according to the figure, its impact is low. This is likely a consequence of the total moist energy norm used to calculate forecast errors: the norm weights are largely focused in the troposphere and are thus bound to ignore impact in the stratosphere (see Todling 2013). In the late 1990s the impact of MSU is reduced as AMSU-A gets in the mix. When the AIRS instrument comes in, the impact of AMSU-A seems to decrease (2002-2008); its impact seems to decrease even further when IASI is introduced (circa 2008), with the impact of AMSU-A becoming comparable with that of AIRS and IASI toward the end of the time series. Though these instruments observe different parts of the spectrum (MW and IR), the improvement any of them brings to the assimilation is retained during the cycle, as an improvement to the background, with the consequence of evening out the contribution of many of the global instruments. All other instruments seem to have much smaller impact in reducing errors in the forecast.

Figure 4. Bubble plot of monthly mean total observation impact of main radiance instruments used in MERRA-2. The bullet size is proportional to the monthly mean observation count. The units of energy are $J\ kg^{-1}$.

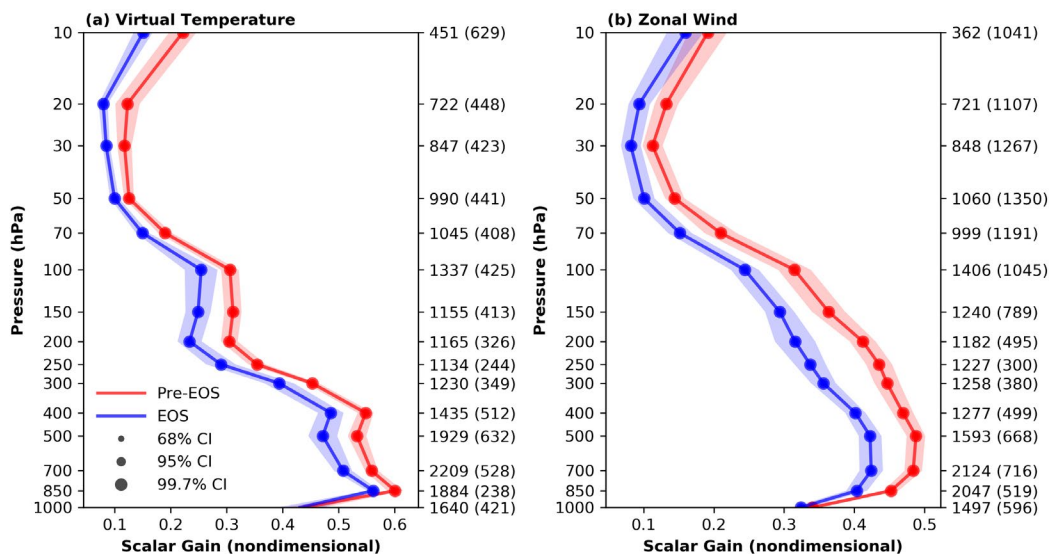


An important fact to remember about MERRA-2 is that it relies on a 3D-Var algorithm with prescribed, fixed, observation, and background error covariances for the whole course of its integration. Indeed, MERRA-2 is derived from GMAO's Forward Processing, near-real-time system. The prescribed errors of this system are tuned to provide best results over the current period, and therefore, one might expect the system to perform less optimally over other periods. The only quasi-adaptive feature of the MERRA-2 3D-Var is its online variational bias correction (Derber and Wu, 1998) and an offline aircraft bias correction procedure. These, however, adjust biases in satellite radiances and aircraft temperature observations but not observation and background error covariances. An illustration of the difference in tuning is provided in *Figure 5*, where scalar analysis gains derived from observation residuals of radiosonde temperature and winds are shown for the pre-EOS and EOS era of MERRA-2. These quantities are constructed from estimates of

background and observation error standard deviation over the eighteen years of January and July months preceding the EOS era (1982-1999) and during the EOS era (2000-2017). If we assume the system to be tuned for the current (EOS) era, the results in the figure suggest the errors associated with the pre-EOS era to be in need of tuning (i.e., requiring an adjustment of the prescribed statistics).

The results here are only a small sample of the amount of information that can be extracted from FSOI as applied to reanalysis. One must bear in mind that conclusions from such studies are considerably dependent on the error metric employed. Final results on this work will soon appear in refereed publication. The next GMAO reanalysis will certainly employ a variational-ensemble hybrid strategy, and such approach is expected to provide a more adaptable error statistics and hopefully ameliorate the weakness of the fixed prescribed statistics in MERRA-2.

Figure 5. Vertical profile of estimates of Kalman gain, $\sigma_b^2/(\sigma_b^2+\sigma_o^2)$, in observation-space for (a) radiosonde residuals of virtual temperature and (b) zonal wind obtained for the 0000 UTC analyses of the January and July months of the pre-EOS (1982-1999; red) and the EOS (2000-2017; blue) eras. Curves represent mean values; shading represents ± 1 standard deviation from the mean. The column on the right represents mean number of observations per cycle in a particular layer for the pre-EOS era and in parenthesis the differences from the pre-EOS era.



Authors

Fabio Diniz, Centro de Previsão de Tempo e Estudos Climáticos (CPTEC), INPE, Brazil

Ricardo Todling, Global Modeling and Assimilation Office (GMAO), NASA, USA

References

Dee, D. P., and S. Uppala, 2009: Variational bias correction of satellite radiance data in the ERA-Interim reanalysis. *Q. J. Roy. Meteor. Soc.*, 135 (644), 1830–1841.

Derber, J. C., and W.-S. Wu, 1998: The use of TOVS cloud-cleared radiances in the NCEP SSI analysis system. *Mon. Wea. Rev.*, 126 (8), 2287–2299.

Gelaro, R., and Coauthors, 2017: The modern-era retrospective analysis for research and applications, version 2 (MERRA-2). *J. Climate*, 30 (14), 5419–5454.

Holdaway, D., R. Errico, R. Gelaro, and J. G. Kim, 2013: Inclusion of linearized moist physics in NASA's Goddard Earth observing system data assimilation tools. *Mon. Wea. Rev.*, 142 (1), 414–433.

Kleist, D. T., D. F. Parrish, J. C. Derber, R. Treadon, W.-S. Wu, and S. Lord, 2009: Introduction of the GSI into the NCEP global data assimilation system. *Wea. Forecast.*, 24 (6), 1691–1705.

Langland, R. H., and N. L. Baker, 2004: Estimation of observation impact using the NRL atmospheric variational data assimilation adjoint system. *Tellus A*, 56 (3), 189–201.

McCarty, W., L. Coy, R. Gelaro, A. Huang, D. Merkova, E. B. Smith, M. Sienkiewicz, and K. Wargan, 2016: MERRA-2 input observations: summary and assessment. Technical Report Series on Global Modeling and Data Assimilation, Volume 46 NASA/TM-2016-104606/Vol. 46, NASA Goddard Space Flight Center, Greenbelt, MD, USA.

Rienecker, M. M., and Coauthors, 2011: MERRA: NASA's modern-era retrospective analysis for research and applications. *J. Climate*, 24 (14), 3624–3648.

Trémolet, Y., 2008: Computation of observation sensitivity and observation impact in incremental variational data assimilation. *Tellus A*, 60A, 964–978.

Todling, R., 2013: Comparing two approaches for assessing observation impact. *Mon. Wea. Rev.*, 141 (5), 1484–1505.

Demonstration of C++ Implementation of GNSS-RO Forward Operators

Introduction

As explained in the previous issue of this newsletter series, Radio Occultation measurement based on Global Navigation System Satellites (GNSS-RO), such as GPS, GLONASS, and Galileo, is a remote sensing technique for atmospheric limb sounding (Fjeldbo 1971, Melbourne 1994, Kursinski 1997 and Gleisner 2013) and retrieval of atmospheric properties, such as temperature, pressure, and humidity profiles. The mathematical theory behind the evaluation of radio occultation signals is quite elegant (Fjeldbo 1971), and has been applied in many operational GNSS-RO forward operators, as well as the Joint Effort for Data Assimilation Integration (JEDI) system currently being developed by the JCSDA (Shao et al., 2019).

The purpose of this short communication is to provide an overview on how to implement this theory in the C++ programming language (Stroustrup 1997). While research implementations of these methods already exist in Fortran, the motivation for advancing to C++ is clear. The consequent implementation of the Object-Oriented Programming (OOP) paradigm and C++'s template system drastically simplifies cooperation on and maintenance and extension of larger code bases compared to Fortran without sacrificing runtime speed, which is important in the context of the JCSDA. Moreover, connecting GNSS-RO algorithms as Unified Forward Operators (UFOs) to the Joint Effort on Data Assimilation Integration (JEDI) framework (Trémolet 2019) is also simplified, and potential for error is reduced since the architecture and class structure of JEDI are implemented in C++ as well.

The implementation of a selection of GNSS-RO operators will be discussed. Section 2 describes the Abel transform approach, while the more general ray tracing approach is considered in Section 3. All the C++ implementations discussed consist of only minimal proof-of-concept codes and are not included in actual data assimilation frameworks.

The Abel Transform

The Abel transform is an integral equation formulated by Norwegian mathematician Niels Henrik Abel (Abel 1826) to describe the falling motion of a point mass. For the simplified case of a cylindrically symmetric atmosphere, the Abel transform can be used to invert the refractive index profile from the GNSS signal bending angle (Fjeldbo 1971):

$$(1) \quad \ln(n(a)) = \frac{1}{\pi} \cdot \int_a^{\infty} \frac{\alpha(x)}{\sqrt{x^2 - a^2}} dx$$

where n is the refractive index profile of the atmosphere, a the impact parameter of the light ray, and α the bending angle of the GNSS signal. In order to evaluate the integral in *Equation 1* for an arbitrary α , a quadrature scheme needs to be chosen. In the current naïve implementation, the exp-sinh quadrature is chosen, which is a double-exponential quadrature scheme (Takahasi 1974) suitable for positive half-infinite intervals.

An important aspect of efficient C++ programming is using suitable and well-tested libraries to avoid reinventing the wheel in a figurative sense. A widely used collection of algorithms and data structures in C++ is the so-called [boost library](#). Features first implemented in boost often find their way in the C++ standard library. As boost already contains an implementation of the exp-sinh quadrature, it is not necessary to repeat the coding of this quadrature scheme here. In order to use the quadrature scheme, it is only necessary to include the corresponding boost header file, as shown in *Listing 1*.

Listing 1. Including a static library header file in C++.

```
#include <iostream>
#include <boost/math/quadrature/exp_sinh.hpp>
```

Listing 2. The return type of the Abel function and the type of its input argument is the template parameter T .

```
template<typename T>
T Abel(T a)
{
    ...
}
```

Listing 3. Defining the integrand as a lambda function.

```
auto integrand = [alpha,a](T x)
{
    return alpha/sqrt(x*x+std::numeric_limits<double>::epsilon() - a*a);
};
```

For the sake of simplicity, the Abel transform is implemented as a function here. C++ functions largely work the same way as their familiar Fortran versions. In order to have a more flexible implementation however, the Abel transform will accept and return a template argument; that is, the return type of the function and its input arguments is determined by the compiler. (*Listing 2*) In this way, the return type of the function can be changed without having to write a separate implementation of the function for each type.

The output type of the function Abel can now be any arbitrary class that implements the necessary algebra, including float, double, vectors, matrices, quaternions, and so on. The integrand of *Equation 1* can be passed to quadrature method as a lambda function (*Listing 3*), which is a (usually short) anonymous function that can be defined locally. This is an advanced feature introduced in the C++11 standard.

Finally, in order to compute the integral, the quadrature method is instantiated as an object of class `exp_sinh` (*Listing 4*), and the integrand is passed to the `integrate(-)` method of the object *integrator*.

This completes a very basic implementation of the Abel transform method in C++.

Hamiltonian Optics

A more general but also more expensive approach to computing the path of the GNSS-RO signal is ray tracing (Fjeldbo 1971). The assumption of a circularly symmetric refractive index profile is not needed anymore, and the method is indeed very general. This is possible because the wavelength of the GNSS signal is very small in relation to all other length scales of the problem. Under these circumstances, the GNSS-RO problem can be described as a Hamiltonian system (i.e., the ray trajectory x and the wave vector k of the ray are functions of a single scalar function only, namely the Hamiltonian H , which can be identified as the total energy of the system) (Ott 2002 and Stegmann 2016).

$$(2) \quad \begin{aligned} \frac{dx}{dt} &= \frac{\partial H}{\partial k} \\ \frac{dk}{dt} &= -\frac{\partial H}{\partial x} \end{aligned}$$

Listing 4. Instantiation of an object of class `exp_sinh`.

```
boost::math::quadrature::exp_sinh<T> integrator;
double termination = sqrt(std::numeric_limits<double>::epsilon());
double error;
double L1;
return exp(integrator.integrate(integrand,
                                a,
                                boost::math::tools::max_value<double>(),
                                termination,
                                &error,
                                &L1 )/M_PI);
```

The system itself has the property that it is symplectic (i.e., the volume of a phase space element $\omega = dx \wedge dk$ is conserved by the system's mapping and the light rays are the path that minimizes the optical length between sender and receiver, which is a function of the refractive index profile). In order to solve *Equation 2* numerically, an ODE solver algorithm is required. In particular, it is highly desirable to use an integrator that retains the symplectic property (Ruth 1983) of the *Equation 2* instead of e.g., conventional Runge-Kutta methods.

For the practical implementation, we again rely on the boost library, specifically its `odeint` component. This is a library that contains a broad range of ODE solvers for many kinds of problems.

Looking at *Equation 2*, the split nature of the ODE in terms of the ray trajectory and wave vector is obvious. Consequently, the RHS functions of *Equation 2* are implemented as two different functions in the code. (*Listings 5 and 6*)

As a matter of fact, the RHS of *Equation 2* is now not implemented as a function anymore, but as a functor or function object. As the name implies, a functor is a class object

Listing 5. Ray trajectory functor implementation.

```

//[ coordinate_function
struct ray_coor
{
    ray_coor(){ }

    void operator()( const container_type &p , container_type &dqdt ) const
    {
        for( size_t i=0 ; i<n ; ++i )
            dqdt[i] = p[i];
    }
};
//[

```

Listing 6. Wave vector functor implementation.

```

//[ momentum_function
struct ray_momentum
{
    ray_momentum(){ }

    void operator()( const container_type &q , container_type &dpdt ) const
    {
        const size_t n = q.size();
        for( size_t i=0 ; i<n ; ++i )
        {
            dpdt[i].m_val[0] = -1.0*q[i].m_val[0];
            dpdt[i].m_val[1] = -1.0*q[i].m_val[1];
        }
    }
};

```

(Barton 1994) with an overloaded input(-) operator and is a common programming construct in C++. As a specific simple test case, the Luneburg lens refractive index profile has been chosen here:

$$(3) \quad n(r) = \sqrt{2 - r^2}$$

After implementing the RHS of *Equation 2*, an ODE solver type needs to be selected. This is done in *Listing 7*. A symplectic solver is selected as the stepper_type (*Listing 7*) and passed to the integrate_const function provided by boost odeint.

Sample output of the ODE integration is presented in *Figure 1*. The image shows a single ray trajectory curving back in on itself and moves around the center of the coordinate system on a stable orbit. As the light ray cannot leave the Luneburg lens, it effectively acts as a black hole.

Summary and Future Plans

As discussed in the previous newsletter (Shao et al., 2019), the JEDI system being developed at the JCSDA adopts the operators from the existing operating systems, written in Fortran. However, the goal of the GNSS-RO work at the JCSDA is to develop a GNSS-RO operator with both

Listing 7. Integration of the ODE with constant step width.

```

//[ integration_GPS_signal
typedef symplectic_rkn_sb3a_mclachlan< container_type > stepper_type;
const double dt = 0.1;

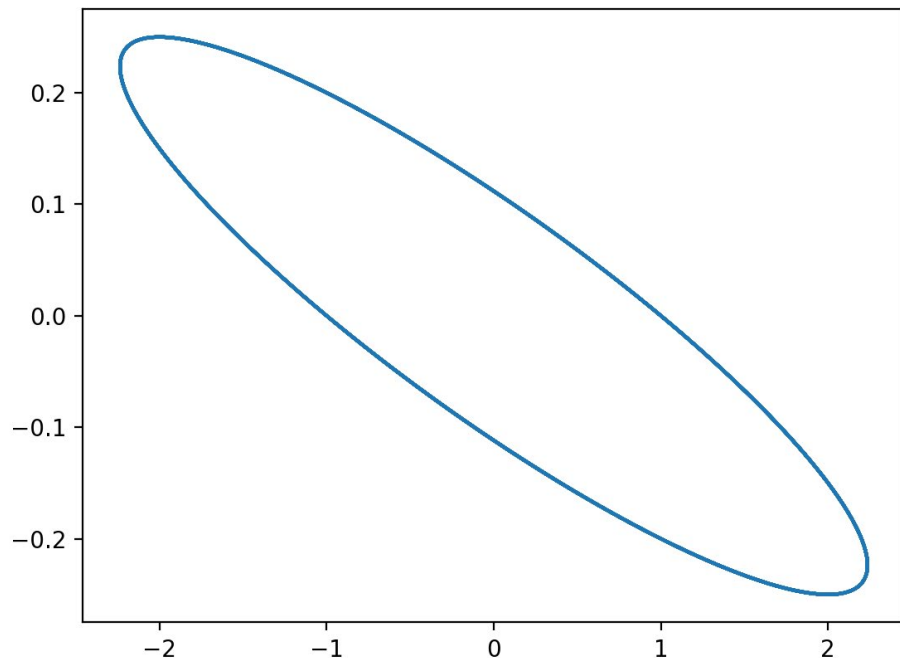
integrate_const(
    stepper_type() ,
    make_pair( ray_coor( ) , ray_momentum( ) ) ,
    make_pair( boost::ref( q ) , boost::ref( p ) ) ,
    0.0 , 50.0 , dt , streaming_observer( cout ) );
//]

```

scientific and computational advancements. This article demonstrates an alternative to current implementations of GNSS-RO operators using modern high-level programming languages (e.g., C++ in this article), as well as carefully selected modern mathematical programming libraries. This is the first step to explore the possibility to advance the GNSS-RO assimilation through alternative computational implementation. Using C++, the essential parts of two types of bending angle forward operators were

successfully implemented, either in a form of an Abel inversion or through solving the ray trajectory equation in an idealized refractivity environment. While the real atmospheric properties will complicate such an implementation, the results certainly are promising. The JCSDA will further investigate feasibility and sufficiency of such an implementation for GNSS-RO with a goal of improving the use of observations and eventually improving numerical weather forecasts.

Figure 1. Ray trajectory for the Luneburg lens profile Equation 3.



Authors

Patrick G. Stegmann (JCSDA), Benjamin T. Johnson (JCSDA) and Hui Shao (JCSDA) stegmann@ucar.edu

Acknowledgements

Funding for this project was provided by the JCSDA partners, including NOAA, NASA, and the Department of Defense, and is gratefully acknowledged. Calculations were carried out at the S4 Supercomputing Facilities of the University of Wisconsin Madison, and the authors gratefully acknowledge the facility staff for their help and assistance, particularly creating a boost module from scratch.

References

Fjeldbo, G., A. J. Kliore, and R. Eshleman (1971): The Neutral Atmosphere of Venus as Studied with the Mariner V Radio Occultation Experiments. *Astr. J.* 76(2), 123-140.

Melbourne, W. G., E. S. Davis, G. A. Hajj, K. R. Hardy et al. (1994) : Application of Spaceborne GPS to Atmospheric Limb Sounding and Global Change Monitoring. JPL Publication 94-18.

Kursinski, E. R., G. A. Hajj, J. T. Schofield, R. P. Linfield, and K. R. Hardy (1997): Observing Earth's atmosphere with radio occultation measurements using the Global Positioning System. *J. Geophys. Res.* 102(D19), 23429-23456.

Gleisner, H. and S. B. Healy (2013): A simplified approach for generating GNSS radio occultation refractivity climatologies. *Atmos. Meas. Tech.* 6, 121-129.

Shao, H., F. Vandenberghe, H. Zhang, B. Ruston, S. Healy, and L. Cucurull (2019): Development of GNSS-RO Operators for JEDI/UFO. JCSDA Quarterly Newsletter 62, DOI:10.25923/w2dh-ep66.

Stroustrup, B. (1997): *The C++ Programming Language* (Third Ed.). ISBN 0-201-88954-4.

Trémolet, Y. (2019): The Joint Effort for Data Assimilation Integration (JEDI). Seventh AMS Symposium on the Joint Center for Satellite Data Assimilation.

Abel, N. H. (1826). *Journal für die reine und angewandte Mathematik* 1, 153-57.

Takahasi, H., and M. Mori (1974): Double Exponential Formulas for Numerical Integration. *Publ. Res. Inst. Math. Sci.* 9(3), 721-741.

<https://www.boost.org> (Retrieved 2019-04-14).

Ott, E. (2002): *Chaos in Dynamical Systems* (Second Ed.). Cambridge University Press.

Stegmann, P. G. (2016): *Light Scattering by Non-Spherical Particles*. Dissertation. URN urn:nbn:de:tuda-tuprints-52570.

Ruth, R. D. (1983): A canonical integration technique. *IEEE Trans. Nucl. Sci.* NS-30(4), 2669-2671.

Barton, J. J., and L. R. Nackman (1994): *Scientific and Engineering C++: An Introduction with Advanced Techniques and Examples*. Addison Wesley Longman Inc., Boston.

MEETING REPORT

*Dr. Yannick Trémolet
presenting at the 2019 IODA
Workshop.*

2019 IODA Workshop Summary



The Interface for Observation Data Access (IODA) is a component of the Joint Effort for Data assimilation Integration (JEDI) software system. From a user's perspective, IODA handles the input of observation data and output of diagnostic data. Efforts to transform IODA from a prototype system into an operational system that can handle big data is under way, and the task of collecting requirements from the Joint Center for Satellite Data Assimilation (JCSDA) partner organizations was initiated by the 2019 IODA Workshop. The workshop took place from February 11 - 13, 2019, in Monterey, California, and was attended by representatives from the U.S. Navy, NOAA, NASA, ECMWF, UK Met Office, NCAR, UCAR, and JCSDA. In total, 41 people attended from 8 partner organizations.

The workshop opened on Monday (February 11th) with introductory remarks from two of the organizers Nancy Baker (NRL) and Yannick Trémolet (JCSDA). These talks were followed by speakers from the Navy, NOAA, NASA, ECMWF, and the UK Met Office describing requirements for observation handling from their various perspectives. The opening presentations were very informative and provided useful requirements information for IODA along with an effective foundation for the focused discussions that were to take place through the remainder of the workshop.

Three focused discussion sessions were conducted over the remainder of the workshop. Tuesday's topics were "In-Memory Observation Handling" and "File and I/O Requirements for Observation Handling." The third discussion session took place on Wednesday with the subject "Pre- and Post-processing Diagnostics Requirements." Each discussion session was preceded by a set of talks given by representatives from the various partner organizations, which served to prepare everyone for the associated discussion. Each set of talks were designed to allow the audience to hear from multiple perspectives including users of DA systems, scientist contributors to JEDI, and JEDI software developers. Material from the presentations was condensed, on the fly, into a list of prompts that were used to seed the subsequent discussion. Workshop participants attended all of the discussion sessions resulting in an effective means for communicating requirements and perspectives among the different partner organizations in the JEDI project.

Work is under way to compile the requirements gathered at the workshop and transform these into the necessary actions to satisfy them. The compilation step has yielded categories that represent different aspects of the IODA design. These categories include themes such as security (the need to handle classified and private data), reliability (an operational system needs to be running 24/7), ease of use, and portability (runs with a variety of hardware platforms, software compilers, and programming languages). We will be using agile software development practices, such as ZenHub tracking and code sprints, to implement solutions for the IODA

requirements. The results of the compilation of requirements along with the tracking of the work will be posted where they can be viewed by the partner organizations.

Overall, the workshop was conducted in a highly positive and enthusiastic manner that solidly reflected the collaborative spirit of the JEDI project. People from different organizations showed up with the intention of shaping IODA into a world-class observation handling system. Many important details relevant to the IODA design and architecture surfaced during the time spent together. We mention here only a few highlights. Although the Human Genome Project is famous for its dealing with big data, the amount of observation data that we are dealing with is roughly an order of magnitude larger. When you consider the model data that are also involved in DA flows, that difference becomes three times greater. The manner in which observation data is collected, organized, and stored in files is incredibly diverse; yet, there appears to be real promise in creating a common method, or a very small set of methods, for organizing and storing those data within IODA. Attaining a common method of organizing and storing the vast amounts of observation data will go a long way in fostering the collaboration, exchange, and sharing of scientific results.

The persistence and resourcefulness of the workshop participants were put to the test Wednesday morning when a wind storm knocked out the power and internet at the meeting site and surrounding neighborhood. Within an hour, communication between on-site and off-site participants was restored using a cell-phone and Bluetooth speaker,

with local participants clustered around laptops, allowing the day's presentations and discussion session to be completed on time. This is a further testament to the collaborative spirit and can-do attitude of the partner organizations.

Monterey proved to be a wonderful venue for the workshop. Many fabulous restaurants and sights to see were at our disposal, including the world-famous Monterey Aquarium and the beautiful sights along the Pacific Coast Highway.

Thanks are due to the organizers of the workshop: Thomas Auligne (JCSDA), Nancy Baker (NRL) and Yannick Trémolet (JCSDA); moderators of the discussion session: Daryl Kleist (NOAA), Ron Gelaro (NASA), Nancy Baker (NRL), and all of the participants who contributed presentations and commentary. Special thanks go to Katherine Shanahan (JCSDA) who handled all of the necessary logistics for the workshop (including a last-minute venue change required as a consequence of the government shutdown), as well as Ben Ruston (NRL) and Elizabeth Satterfield (NRL) who organized the social activities that built the camaraderie of the group. The organizers and the JEDI team are grateful to all participants for making the 2019 IODA Workshop remarkably successful, productive, and enjoyable.

Workshop summary was provided by Stephen Herbener.

PEOPLE

Dr. Maryam Abdi-Oskouei



Dr. Maryam Abdi-Oskouei joined JCSDA and NCAR/MMM in Boulder in January 2019. She is on the core team for the Joint Effort for Data Assimilation Integration (JEDI) project. Maryam is working on developing unit testing for JEDI, WRF model, and MPAS model. Maryam received her PhD in environmental engineering with a focus on atmospheric modeling from the University of Iowa. Her thesis focuses on using various suites of measurements along with data assimilation techniques to reduce the uncertainties in the Chemical Transport Models (CTMs) and emission estimates. Maryam previously collaborated with NCAR/ACOM scientist to improve the emission estimates from oil and gas extraction sites in Colorado using measurements from the FRAPPÉ field campaign. During her PhD, she participated in several field campaigns, such as Lake Michigan Ozone Study (LMOS), ObseRvations of Aerosols above CLouds and their intERactionS (ORACLES), and Korea US Air Quality Study (KORUS-AQ) as an air quality modeler. Besides modeling and programming, Maryam is a nature enthusiast and an animal lover. She enjoys spending time in the mountains and hiking with her dog. She also enjoys astrophotography, spending many nights outdoors trying to capture the beauty of the universe.



James Rosinski

James Rosinski has been with the JCSDA in Boulder since July, 2018. Hired as a visiting scientist, James' primary role is working with Ben Johnson and other scientists on the CRTM radiative transfer model. A major focus of James' work is modifying the CRTM code for optimal efficiency when run on supercomputing platforms such as NOAA's "Theia" machine and NCAR's "Cheyenne." One milestone reached so far is the ability to use multiple CPU cores on a single node of these machines to speed up the calculations. The implementation mechanism was OpenMP threading. Faster computation is important for applications such as the GSI data assimilation (DA) package, which uses the CRTM and must complete a DA cycle within a very narrow time window.

The CRTM is also a component of the JEDI software infrastructure project. As such, James is busy becoming familiar and working with JEDI and the implementation of CRTM within it.

Since James' appointment is half-time, he has a fair amount of time for other activities. This summer James completed a third semester Spanish class at Front Range Community College in Longmont. He also likes to travel, enjoys hiking, snowshoeing, and other outdoor activities.



Kat Shanahan

Kat Shanahan joined the JCSDA Boulder team in October 2018. She provides administrative and logistical support for on- and off-site JCSDA staff. Her main duties include meeting planning, new hire onboarding, travel support, and website management. She is excited to be part of a growing center of excellence!

Before joining the JCSDA, Kat attended Indiana University for her M.S.Ed. in Learning Sciences and the University of Colorado, Boulder for her B.A. in Astrophysics. Her graduate research work focused on a collaborative game-based learning project where she generated content and educational design to help middle school students investigate the phenomenon of eutrophication. As an undergraduate, she worked as a research assistant reducing astronomical data to study transient objects and Luminous Blue Variable (LBV) stars. Kat is passionate about planetary science, science education, and astronomy educational outreach. She has worked many open houses at observatories in both Colorado and Indiana.

In her spare time, Kat enjoys painting, hiking, running, reading up on quantum mechanics, and listening to music.



Dr. Anna Shlyaeva

Dr. Anna Shlyaeva joined JCSDA in November 2018, as a part-time software engineer in the Joint Effort for Data assimilation Integration (JEDI) development team. With JEDI, Anna is working on the generic aspects of forward operators and ensemble data assimilation algorithms. She also provides support to people implementing observation operators in JEDI.

Anna graduated from Moscow State Technical University in Russia, with a PhD in Computer Science. She has been interested in applied mathematics for atmospheric sciences since her undergrad studies when she worked at the Hydrometeorological Center of Russia. There, she worked for almost 10 years on various data assimilation projects, including developing ensemble data assimilation system for the global NWP from scratch. At the same time, she worked at the Technical University in Moscow as an assistant professor, teaching at the Software Engineering Department.

After juggling two jobs in Moscow, Anna spent two years at the Canadian Meteorological Center in Montreal, working on the ensemble data assimilation for sea ice application. Having grown up in the Far East of Russia close to the Arctic Circle, she was the only sea ice data assimilation team member who had actually seen sea ice. Anna hopes to get back to doing more work on sea ice and the Arctic.

Anna moved to Boulder, Colorado, in 2015, to share home and life with her husband, daughter, and stepsons. She started a job as a research scientist with NOAA at that time, where she still works part-time on the ensemble data assimilation aspects and production of the global atmospheric ensemble reanalysis.

Anna loves watching sunrises with a cup of coffee and a toddler pointing out all the colors in the sky, traveling and seeing new places, reading, enjoying visual arts, and would like to do more photography and hiking.

EDITOR'S NOTE

Colleagues,

April 1, 2019 marked the beginning of the JCSDA Fiscal Year 2019, and it was gratifying to have the Annual Operating Plan completed and approved by the Management Oversight Board and begin to execute the plan on schedule. The AOP incorporates the work to be performed by the Core “in-kind” staff who are dedicating a portion of their effort to support JCSDA Projects and tasks and achieving the milestones associated with them.

An exciting and challenging aspect of this year’s plan is the recruitment and on-boarding of qualified new staff to address an expanded workload. An All-Hands Tele-meeting was conducted on April 4, 2019, to review the AOP, the staff roles and responsibilities, goals for the year, and to answer questions and concerns for new staff and long-time participants alike. In this issue of the Newsletter, you will find short biographies to introduce several new JCSDA colleagues: Dr. Anna Shlyaeva, Ms. Kat Shanahan, Mr. Jim Rosinski, and Dr. Maryam Abdi-Oskouei. I hope you’ll take time to learn a little about them from these pages, and that you will have the chance to welcome them and get to know them better in the course of working together.

Although the tasks have evolved as a result of the accomplishments of the previous years and the evolving needs of the JCSDA partners, the Projects under which they are organized remain familiar, for example, the Community Radiative Transfer Model (CRTM), which has been central to the JCSDA since its inception. In this issue, Dr. Emily Liu of NCEP’s Environmental Modeling Center (EMC) and her co-authors have contributed an article describing some of EMC’s contributions to the development and validation of the CRTM for a variety of IR and MW sensors. The article underscores the cooperation of EMC and NESDIS/STAR working with JCSDA Core staff to develop and test improved elements of the CRTM, and the establishment of validation procedures that can be re-used as progressively more challenging RT targets - precipitating MW, all-sky IR radiances, etc., are tackled.

Dr. Ricardo Todling of NASA’s Global Modeling and Assimilation Office (GMAO) and his co-author, Fabio Diniz, have provided an instructive article on the use of Forecast Sensitivity Observation Impact (FSOI) to support a 40-year reanalysis project providing a means of assessing the contributions of all constituents of the observing system efficiently, within the limits they describe, and setting the stage for a performing a subsequent reanalysis using more adaptable error statistics than in the present case.

JCSDA’s Dr. Patrick Stegmann and his co-authors have contributed an article to this edition on the coding of C++ GNSS RO Forward Operators, facilitating their use via JEDI. During his recent stay as a visiting scientist at the Remote Sensing Products division at EUMETSAT

headquarters in Darmstadt and the Data Assimilation group of the German Weather Service, Patrick was approached by the press team of his alma mater, the Technical University of Darmstadt, to be interviewed about his work at the JCSDA. [A summary of the interview](#) (in German) has been published in the news magazine of the TU Darmstadt as part of a series on distinguished alumni working in the United States.

Finally, I draw your attention to one upcoming event, the JCSDA Symposium at the 100th Annual Meeting of American Meteorological Society in Boston next January. The call for papers will be out this Summer; please keep an eye out for it and consider submitting your contribution.

Jim Yoe

SCIENCE CALENDAR

UPCOMING EVENTS

MEETINGS OF INTEREST

DATE	LOCATIONS	WEBSITE	TITLE
July 28–August 2, 2019	Singapore	http://www.asiaoceania.org/aogs2019/public.asp?page=home.htm	16th Annual Meeting Asia Oceania Geosciences Society (AOGS)
July 28–August ,2 2019	Yokohama Japan	https://igarss2019.org/default.asp	IGARSS
September 16-20 2019	Honolulu, HI	http://www.oceanobs19.net/	OceanObs'19
September 28–October 4, 2019	Boston, MA	https://www.ametsoc.org/index.cfm/ams/meetings-events/ams-meetings/2019-joint-satellite-conference/2019-joint-satellite-conference-call-for-papers/?utm_source=Subscribers&utm_medium=Email&utm_campaign=Newsletter&zs=5EW4e1&_zl=cf3a5	Joint AMS/EUMETSAT/NOAA conference
October 31–November 6	Saint-Saveur, Québec, Canada	https://cimss.ssec.wisc.edu/itwg/index.html	TOVS ITSC THE 22nd INTERNATIONAL TOVS STUDY CONFERENCE (ITSC-22)
November 4–8, 2019	Herzliya, Israel	http://www.cospar2019.org/	4th COPSAR Symposium Small satellites for sustainable Science and Development
December 9–13, 2019	San Francisco, California	https://sites.agu.org/	AGU
January 12–16, 2020	Boston, MA	https://www.ametsoc.org/index.cfm/ams/	AMS Annual Meeting
June 2020	Fort Collins, Colorado	TBD	8th International Symposium on Data Assimilation (ISDA)

MEETINGS AND EVENTS SPONSORED BY JCSDA

DATE	LOCATIONS	WEBSITE	TITLE
May or June 2019 (proposed)	Boulder, CO		JEDI Academy 3
October 2019 (proposed)	Monterey, CA (proposed)		JEDI Academy 4

CAREER OPPORTUNITIES

The Joint Center for Satellite Data Assimilation is currently seeking qualified candidates to fill several varied job openings. Descriptions of these positions and directions for applying may be found via the University Corporation for Atmospheric Research the Cooperative Programs for the Advancement of Earth System Science (UCAR/CPAESS) webpage: <https://cpaess.ucar.edu/employment-announcements>.

JOB TITLE	LOCATION
JCSDA Software Engineer II - Obs Storage (19108)	Boulder, Colorado, United States
JCSDA Associate Scientist III - NIO UFO (19112)	Various, United States
JCSDA Project Scientist I - IOS FSOI (19110)	Various, United States
JCSDA Project Scientist I - NIO GIIRS (19116)	Madison, Wisconsin, United States
JCSDA Project Scientist I/II - EMC Liaison (19105)	College Park, Maryland, United States
JCSDA Project Scientist I/II - ESRL Liaison (19107)	Boulder, Colorado, United States
JCSDA Project Scientist I/II - NIO RadDA (19111)	College Park, Maryland, United States
JCSDA Project Scientist II - LandDA (19113)	Various, United States

For a full listing of job openings available for NCAR/UCAR, please visit this [website](#).

Opportunities in support of JCSDA may also be found at <http://www.jcsda.noaa.gov/careers.php> as they become available.